Topical Review

High contrast femtosecond laser-driven intense hard X-ray source for imaging application

L.M. Chen [a,*], W.M. Wang [a], M. Kando [b], L.T. Hudson [c], F. Liu [a], X.X. Lin [a], J.L. Ma [a], Y.T. Li [a], S.V. Bulanov [b], T. Tajima [b], Y. Kato [b], Z.M. Sheng [a,d], J. Zhang [a,d]

[a] Beijing National Laboratory of Condensed Matter Physics, Institute of Physics, CAS, Beijing 100080, China
[b] Advanced Photon Research Center, Japan Atomic Energy Agency, 8-1 Umemidai Kizugawa, Kyoto 619-0215, Japan
[c] National Institute of Standards and Technology, 100 Bureau Dr., Gaithersburg, MD 20899, USA
[d] Department of Physics, Shanghai Jiao Tong University, Shanghai 200240, China

ARTICLE INFO

ABSTRACT

In this report we address the current situation of laser-driven hard X-ray sources for imaging applications, especially the saturation of X-ray conversion efficiency and the serious impact upon imaging quality. By employing high contrast laser pulses, the conversion efficiency to X-rays from solid foil targets is improved and the structure of the spectrum can be optimized with respect to imaging applications. In addition, bright Ar K-shell X-rays with very little continuum background have been generated by irradiating, with an ultra-high contrast laser, a target of Ar gas clusters created by a gas jet. These improvements show great potential for single-shot ultrafast X-ray imaging.

© 2009 Elsevier B.V. All rights reserved.

1. Introduction

The recent availability of intense femtosecond laser pulses [1] has opened a new laser–solid interaction regime in which intense laser pulses are deposited into a solid faster than the hydro-dynamic expansion of the target surface. Hot electrons generated via collective absorption mechanisms such as resonant absorption (RA) [2] or vacuum heating (VH) [3] penetrate into a solid target to produce hard X-rays via K-shell ionization and bremsstrahlung [4]. This new kind of intense and ultrafast laser-driven hard X-ray source (LHXS) has a number of interesting applications for the dynamic probing of matter and in particular medical imaging techniques [5]. The enabling features include micrometer X-ray emission source size, picosecond pulse lengths, compact table-top system size and, of most importance, peak brightness larger than 10^{20} photons/s/mm^2/mrad^2/(0.1% BW), comparable to third generation synchrotron radiation sources.

2. Current status of LHXS

The most important characteristic for LHXS is the conversion efficiency of the laser energy to X-ray energy. The control and optimization of hard X-ray emission produced by high-intensity laser–solid interactions requires a mechanistic understanding of

the following steps: the laser energy absorption channel, hot electron generation and the creation of X-rays. Several groups have already reported X-ray emission experiments generated by sub-picosecond laser systems [6–12]. Previous work [6,7] used hundreds of femtosecond laser pulses produced by CO_2 or Nd laser systems. Here RA was identified as the primary heating mechanism in this regime, optimized by creation of plasma density gradients steepened by the ponderomotive force. Recently, it was shown that the use of laser pulse durations less than 100 fs involves new X-ray emission processes. Eder et al. [8] reported observing a maximum in Kα emission when the target was placed away from best focus and qualitatively explained it with the re-absorption of produced photons inside the target. Based on an optimal scale length for RA, Reich et al. [9] theoretically presented a scaling law to estimate the optimal laser intensity and predicted a reduction of the hard X-ray yield if this laser intensity is exceeded. Zhidkov et al. [10] studied prepulse effects with a low contrast fundamental 42 fs laser due to the presence of amplified spontaneous emission and showed the presence of a large plasma gradient $L=2\,\mu m$ at modest laser intensities. They observed a decrease of the laser energy absorption with shorter pulse durations while maintaining a constant laser energy. This was demonstrated experimentally by Schnürer et al. [11], who reported the critical influence of the plasma gradient for hard X-ray emission via the resonant process. All these publications proved that there is a limitation for hard X-ray enhancement with laser intensity based on RA when tens-of-fs, low contrast lasers are used. Chen et al. [12] have affirmed that RA is not effective in the regime of tens-of-fs laser irradiation
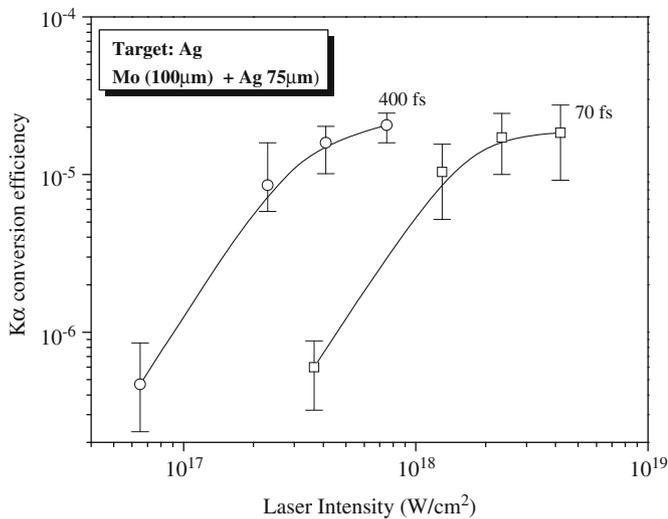
Fig. 1. The Kα conversion efficiency dependence upon laser intensity with the normal laser contrast with either 70 or 400 fs pulse duration.
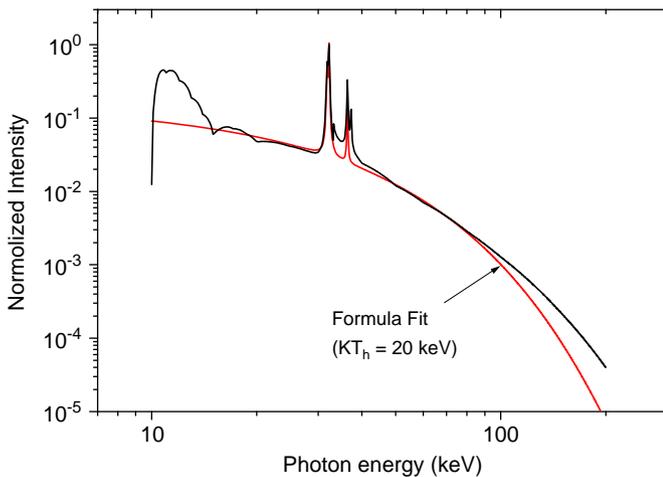

Fig. 2. The experimental LHXS spectrum fitted by the Maxwellian distribution with hot electron temperature kT_h=20 keV.

because the laser pulse duration is too short to effectively stimulate a resonant plasma wave. As Fig. 1 shows, the conversion efficiency from Ag target saturates when the laser intensity is higher than 10^{18} W/cm^2. However, Salzmann [13] summarized the LHXS emission measured in many labs using normal contrast laser pulses, finding that the LHXS is ten times lower than the theoretical prediction. Therefore, new studies are necessary to understand and enhance the conversion efficiency of LHSX in the relativistic regime.

Typically the X-ray continuum in a spectrum is strong and usually contains 90% of the total X-ray energy with photon energies greater than 1 keV [1]. This is harmful to the imaging quality. As shown in Fig. 2, besides the K-shell characteristic line emission, there is a strong continuous background with hot electron temperature kT_h that extends beyond 100 keV. In imaging practice, this hard X-ray flux is passed through a filter to reduce the energetic photon tail, as shown in Fig. 3. However, if the hot electron temperature is too high, the energetic X-ray tail cannot be entirely eliminated. In many cases, this energetic X-ray tail leakage will greatly reduce the subject contrast of in-line radiography. Fig. 4 shows the figure-of-merit simulation data using the FOM code [5] showing how imaging subject contrast decreases with increase in hot electron temperature. In a previous experiment using such a laser source with significant broad background, we found a subject contrast SC=0.24 in a mammography imaging experiment, which is even worse than the case of using a conventional X-ray tube, SC=0.6. This is the most serious challenge for LHXS in imaging applications.

3. Optimization of LHXS from solid targets

The following experiments are realized with the high-intensity Ti:Sapphire laser system in the Laboratory of Optical Physics, Institute of Physics in Beijing, China. The laser delivers a maximum output energy of over 300 mJ per pulse after compression with a pulse duration of 60 fs and a repetition rate of 10 Hz. After compression, the prepulse from 8 ns before the main pulse is 2×10^{-5} of the main pulse monitored using fast photodiode. The laser contrast for a picosecond pedestal obtained using a high-dynamic-range, third-order femtosecond auto-correlator (Sequoia) is 1×10^4. A type I potassium dideuterium phosphate (KDP) frequency doubling crystal (1 mm thick) is used to get the 400 nm second-harmonic pulse. The infrared is rejected by
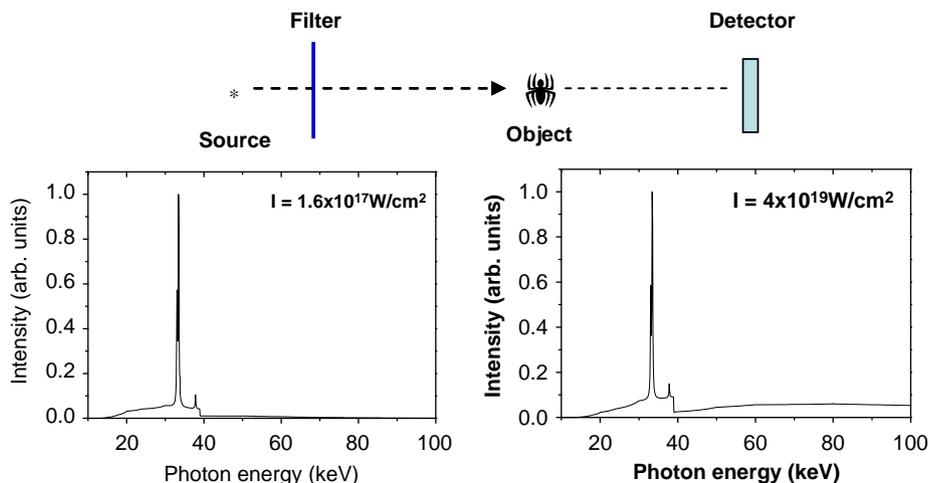

Fig. 3. The geometry of in-line X-ray radiography (upper) and the X-ray spectrum on detector generated by laser with intensity 1.6×10^{17} and 4×10^{18} W/cm^2.
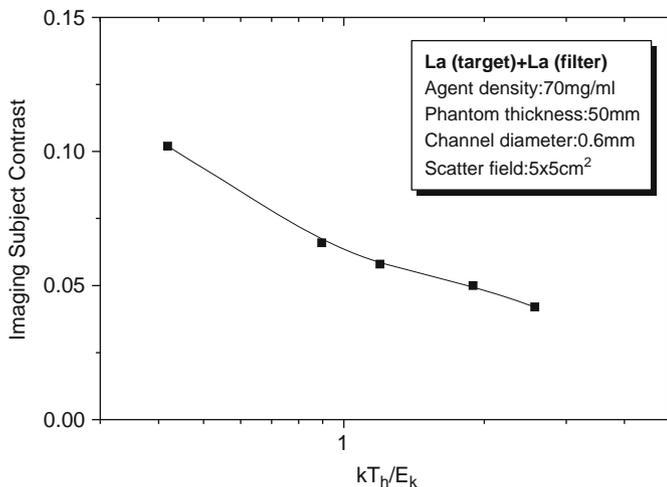
Fig. 4. The simulated imaging subject contrast as a function of the hot electron temperature (E_k is the Kα photon energy).

Table 1
Source parameters in the case of fundamental (800 nm) and frequency-doubled (400 nm) laser pulse irradiation.

	800 (nm)	400 (nm)
Laser contrast in ns	5×10^4	$> 10^9$
Laser contrast in ps	1×10^4	$> 10^8$
Density gradient length (λ)	> 3	< 0.1
KT_h (keV)	> 150	~ 30
X-ray size (μm)	~ 100	~ 15

passing the beam over 4 dielectric-coated mirrors. This increases the pulse contrast ratio compared to the picosecond pedestal over 10^8 and by over 10^9 in the ns time window. Finally, the p-polarized laser pulse is obliquely incident on the target at 45° by an f/3.5 parabola mirror in a focal spot diameter of 10 μm (FWHM) with an average intensity of 1×10^{18} W/cm^2. An Ag foil target with thickness 15 μm was used in the experiments. The measurement of the X-ray spectrum and the determination of the η_K are made with a single photon counting X-ray LCX-CCD camera (Princeton) used as an energy-dispersive spectrometer [6]. The X-ray emission size is measured with the knife-edge imaging technique [6]. The FWHM of a fitted Gaussian distribution function gives an X-ray emission size ~10 μm at 400 nm laser irradiation. It implies no evident plasma expansion in this case. Table 1 shows the experimentally determined parameters obtained using 800 and 400 nm laser pulses.

Fig. 5 presents the Kα conversion efficiency measured using an Ag target with X-ray CCD camera as a function of laser intensity for both 800 nm (dashed line) and 400 nm (solid line) p-polarized laser pulse irradiation. The curve associated with the normal contrast incident laser pulse (800 nm) shows saturation of conversion efficiency as a function of laser intensity; the case of high contrast laser irradiation (400 nm) is not saturating in this regime and scales as $\sim(I)^{5.0}$. The Ag η_K in 2π steradian reaches $\sim 3 \times 10^{-5}$ at the intensity 1×10^{18} W/cm^2, which is 3 times the efficiency achieved using the normal contrast laser. Fitting the X-ray spectrum with a Maxwellian distribution, the hot electron temperature is found to be about 30 keV, and 150 keV for the case of low contrast incident laser irradiation. This implies that the X-ray energetic tail is greatly suppressed in the high contrast case. It should be noted, however, that the X-ray spectrum in the high contrast case is not truly Maxwellian and an evident energy cutoff exists similar to that reported in Ref. [14].
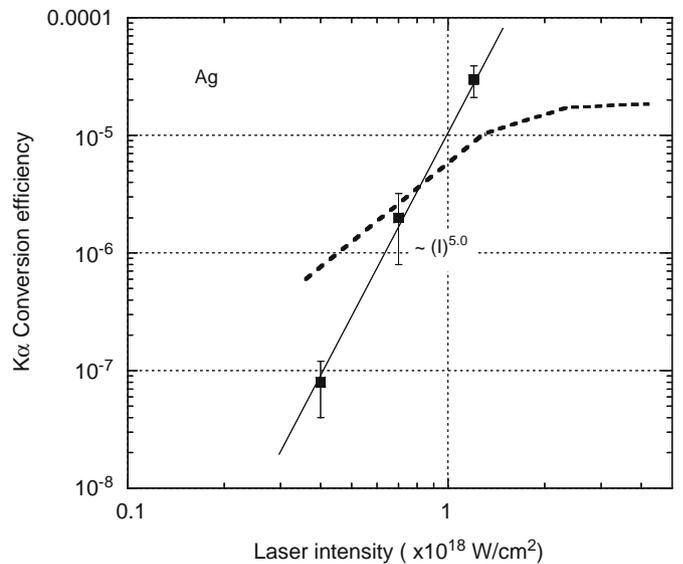

Fig. 5. Kα conversion efficiency as a function of laser intensity in the case of high contrast (solid line) and normal contrast (dashed line) laser pulse irradiation.
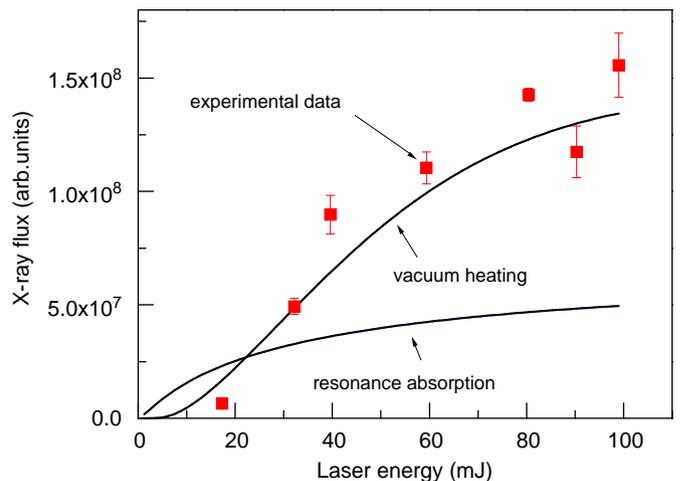

Fig. 6. Experimental data of X-ray photon flux (solid triangle) fitted by VH (solid line) and RA (dashed line) mechanisms.

The vacuum heating (VH) mechanism dominates resonant absorption (RA) mechanism for steep density gradients [3,15]. VH is a mechanism that can occur when a p-polarized light pulse is obliquely incident on an atomically abrupt metal surface; it is strongly absorbed by pulling electrons into the vacuum during an optical cycle, then returning the electrons to the surface with approximately the quiver velocity [3]. With our laser intensity of 1×10^{18} W/cm^2, the plasma scale length L is 0.05λ according to our hydrodynamic calculations and is consistent with Ref. [16], which employed similar conditions. This satisfies the necessary condition to stimulate VH: $X_{osc} \leqslant L$. It also satisfies the optimal condition for VH: $V_{osc}/c \leqslant 3.1(L/\lambda)^2$ [15] in which $V_{osc} = eE/m_e\omega$ is the electron quiver velocity in the laser field that is governed by the quiver energy: $E_q = mc^2[(1+2U_p/mc^2)^{1/2} $ [1], where U_p(eV)$=9.3 \times 10^{-14}I\lambda^2$ is the ponderomotive potential. Experimental data were fitted by assuming the laser–electron interaction is governed by the VH or RA mechanisms separately, as shown in Fig. 6. The VH curve fits very well the experimental result, which indicated it is dominating the RA mechanism in this intensity and contrast regime. The X-ray emission size measured with a knife-edge imaging technique

Fig. 7. Image of mouse tail obtained by using Ag LHXS driven by high contrast laser pulses. The mesh scales as 1 cm.
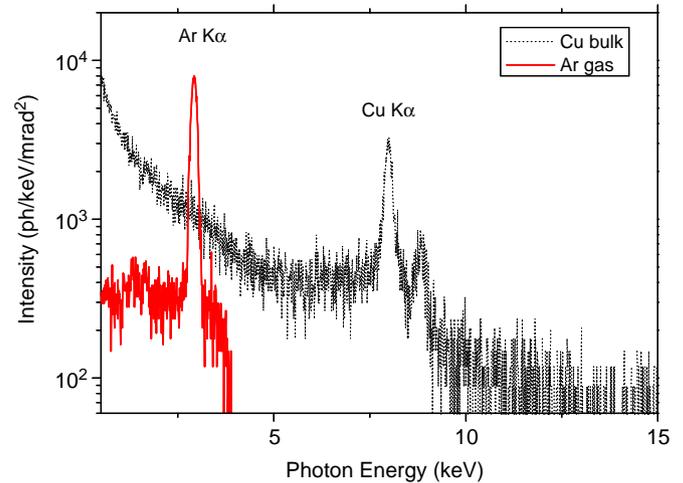

Fig. 8. X-ray spectrum obtained using Ar gas+cluster (solid line) and solid (dashed line) target.
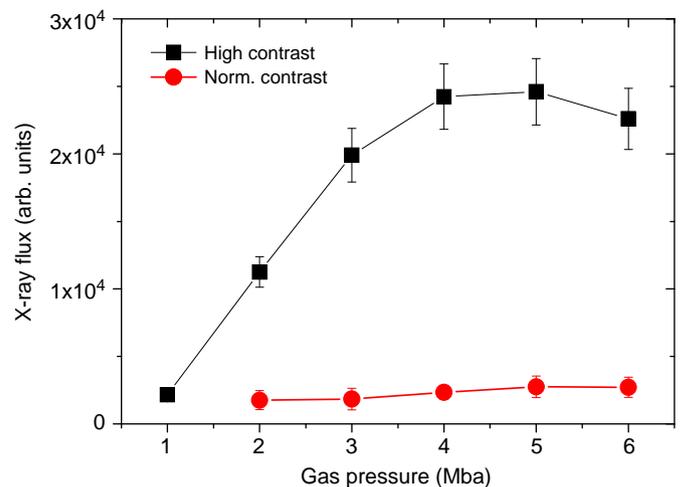

Fig. 9. Ar K-shell X-ray flux depend as a function of gas backing pressure in high contrast (square) and normal contrast (circle) laser irradiation.

confirmed our electron temperature measurement. The X-ray emission size generated by 400 nm laser irradiation was found to be 15 μm. This value is much smaller than in the case of an 800 nm laser pulse, where the size is over 100 μm. Therefore, we conclude VH is stimulated and may be the main absorption mechanism in our experiment.

In-line small-animal radiography is carried out using this intense quasi-monochromatic X-ray source. Fig. 7 shows the absorption-contrast projection image of a mouse tail using a magnification about 2; the detector is Fuji X-ray film backed on the AD M-fine screen. The absorption-contrast image shows very fine structure in detail with a resolution of about 20 μm, which is similar to the X-ray source size.

4. Optimization of LHXS from rare-gas cluster targets

To get a brighter and more monochromatic X-ray source, we present ongoing efforts to produce and measure hard X-ray spectra from an Ar gas+cluster target irradiated by a femtosecond laser pulse at 10^{17} W/cm^2 [17]. As shown in Fig. 8, the spectrum shows a high-contrast characteristic K-shell emission, a suppressed continuum and the elimination of the energetic X-ray tail typically observed with solid target laser irradiation. The integrated K-shell photon power is over 70% of the total hard X-ray-integrated energy in the spectrum. This Ar K-shell X-ray source with very little continuum background was found to possess a flux of 1.2×10^3 photons/mrad^2/pulse. The peak brightness is estimated to be $\sim 1.2 \times 10^{21}$ photons/s/mm^2/mrad^2, which is comparable to third-generation synchrotron radiation sources. This source is critically dependent on the contrast of the incident laser pulse. If the laser contrast is reduced from 10^8 to 10^6, the emitted flux is greatly decreased. In addition, as shown in Fig. 9, the X-ray flux driven by normal contrast laser pulse irradiation does not show a dependence of the gas backing pressure and it is very weak.

Recently, a tenfold X-ray enhancement was obtained [18] wherein the peak brightness reached $\sim 1 \times 10^{22}$ photons/s/mm^2/mrad^2, which was ascribed to a new electron heating mechanism. For the first time, single-shot keV photon phase-contrast-imaging is available which is suited for ultrafast X-ray radiography. This source is shown to have an ultrashort duration ~ 10 fs. It is applicable to a wide variety of investigations requiring ultrafast keV X-rays.

Simulations using a 2D fully electromagnetic particle in cell (PIC) code have been performed, where a linearly polarized laser pulse with sin^2 pulse envelope is launched along the +x direction onto a cluster with a 10-nm diameter and a density of $40n_{cr}$. Fig. 10(a) shows the electron number of inner electrons decreasing with time period but for each half optical cycle, a fraction of electrons will return into the cluster boundary reflecting the electron quiver behavior. These electrons, with quiver energy shown as these small spikes on the curve in Fig. 10(b) and (d), will pass through the cluster and stimulate K-shell ionization to produce X-rays when the electron energy is larger than the Ar ionization threshold. Therefore, we conclude that the K-shell X-ray photon generation arises from electrons quivering in the early stage of intense laser fields. In Fig. 10(d), only 4–5 optical cycles create electron spikes higher than the ionization energy level, and these correspond to the duration about 10 fs. On the other hand, the cluster inner electrons obtain energy much lower than E_k, which leads to no contribution to K-shell ionization in our case, as shown in Fig. 10(c).

This compact quasi-monochromatic X-ray source produced by the irradiation of rare-gas clusters has been applied to X-ray radiographic imaging of biological specimens. For example, with a source size of only 12 μm, a high-resolution phase-contrast image of a spider is shown in Fig. 11.
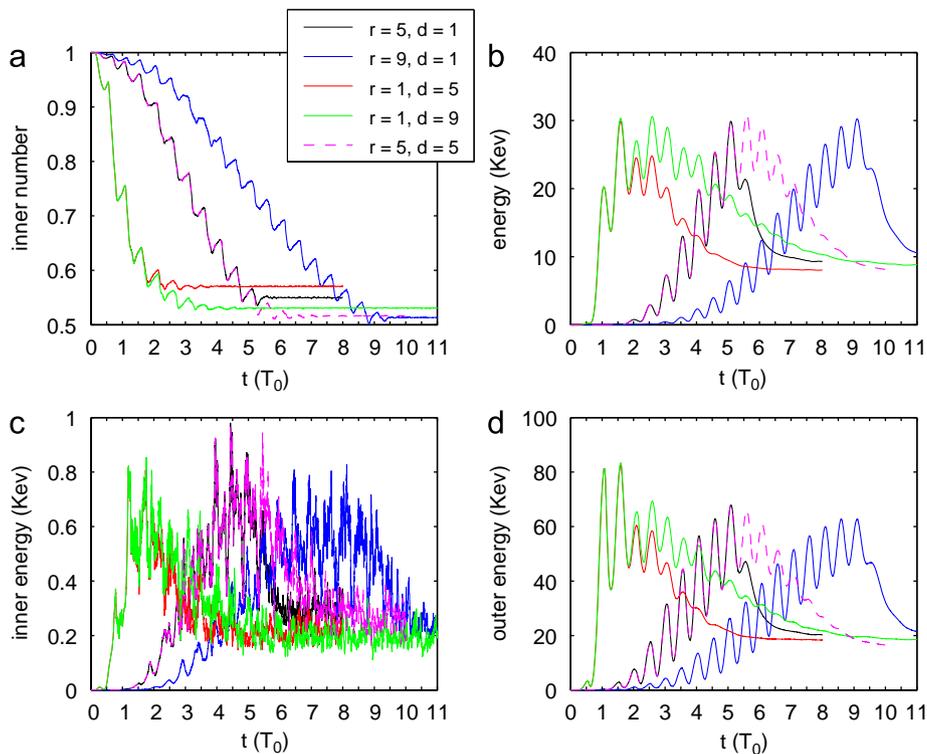
Fig. 10. Temporal distribution of cluster inner electron density (a), electron average energy (b), inner (c) and outer (d) electron average energy in response to various pulse shapes. $I=3.4 \times 10^{17}$ W/cm^2, diameter=10 nm, ne=40. Time unit is in optical cycle.
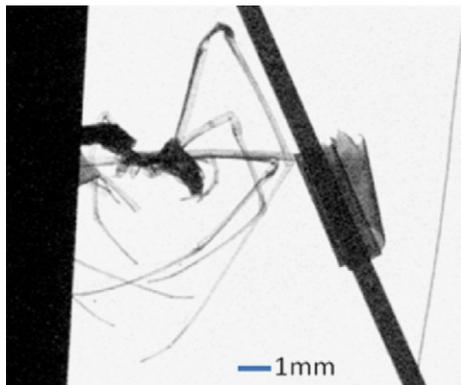
Fig. 11. Phase-contrast imaging of a spider using cluster X-ray source, time-integrated photon flux on detector is 10^6.

5. Summary

The current situation and challenges in producing laser-driven hard X-ray sources for imaging applications are addressed, especially the monochromaticity and saturation of X-ray conversion efficiency, which determine the imaging quality. We introduced high contrast laser pulses which both enhanced the conversion efficiency from solid foil targets and improved the structure of the X-ray spectra. By irradiating a target containing rare-gas clusters of argon with an ultra-high contrast laser, a bright Ar K-shell X-ray spectrum with very little background has been generated with peak brightness of $\sim 1 \times 10^{22}$ photons/s/ mm^2/mrad^2. Applications requiring single-shot ultrafast X-ray imaging are available for the first time. We plan to extend these methods to other rare-gas clusters and use these unique sources to investigate ultrafast phenomena. In addition, working toward a compact hard X-ray free electron laser is a goal of this research.

References

[1] M.D. Perry, G. Mourou, Science 264 (1994) 917;
    D. Strickland, G. Mourou, Opt. Commun. 56 (1985) 219.
[2] W.L. Kruer, The Physics of Laser Plasma Interactions, Addison-Wesley, New York, 1988.
[3] F. Brunel, Phys. Rev. Lett. 59 (1987) 52;
    F. Brunel, Phys. Fluids 31 (1998) 2714.
[4] H. Chen, et al., Phys. Rev. Lett. 70 (1993) 3431;
    T. Feurer, et al., Phys. Rev. E 56 (1997) 4608.
[5] A. Krol, et al., Med. Phys. 24 (5) (1997) 725;
    J.C. Kieffer, A. Krol, Z. Jiang, C. Chamberlain, E. Scalzetti, Z. Ichalalene, Appl. Phys. B 74 (2002) 75.
[6] J. Yu, et al., Phys. Plasmas 6 (4) (1999) 1318.
[7] B. Soom, et al., J. Appl. Phys. 74 (9) (1993) 5372;
    M. Schnurer, et al., J. Appl. Phys. 80 (10) (1996) 5604;
    U. Teubner, et al., Phys. Rev. Lett. 70 (1993) 794.
[8] D.C. Eder, G. Pretzler, E. Fill, K. Eidmann, A. saemann, Appl. Phys. B 70 (2000) 211.
[9] Ch. Reich, P. Gibbon, I. Uschmann, E. Forster, Phys. Rev. Lett. 84 (2000) 4846.
[10] A. Zhidkov, et al., Phys. Rev. E 62 (2000) 7232.
[11] M. Schnürer, et al., Phys. Rev. E 61 (2000) 4394.
[12] L.M. Chen, P. Forget, S. Fourmaux, et al., Phys. Plasmas 11 (9) (2004) 4439.
[13] D. Salzmann, Phys. Rev. E 65 (2002) 036402.
[14] L.M. Chen, et al., Phys. Rev. Lett. 100 (2008) 045004.
[15] P. Gibbon, A.R. Bell, Phys. Rev. Lett. 68 (1992) 1535.
[16] S.C. Wilks, et al., Phys. Rev. Lett. 69 (1992) 1383.
[17] L.M. Chen, et al., Appl. Phys. Lett. 90 (2007) 211501.
[18] L.M. Chen, et al., (arXiv:0907.3421).